# Sleep State Analysis Using Calcium Imaging Data by Non-negative Matrix Factorization

Mizuo Nagayama[1(✉)], Toshimitsu Aritake[1], Hideitsu Hino[2,3], Takeshi Kanda[4], Takehiro Miyazaki[4], Masashi Yanagisawa[4], Shotaro Akaho[3,5], and Noboru Murata[1,3]

[1] Waseda University, Shinjuku, Tokyo 169-0072, Japan
mizuo.n@asagi.waseda.jp
[2] The Institute of Statistical Mathematics, Tachikawa, Tokyo 190-8562, Japan
[3] RIKEN Center for Advanced Intelligence Project, Chuo, Tokyo 103-0027, Japan
[4] University of Tsukuba, Tsukuba, Ibaraki 305-8573, Japan
[5] National Institute of Advanced Industrial Science and Technology, Tsukuba, Ibaraki 305-8568, Japan

**Abstract.** Sleep is an essential process for the survival of animals. However, its phenomenon is poorly understood. To understand the phenomenon of sleep, the analysis should be made from the activities of a large number of cortical neurons. Calcium imaging is a recently developed technique that can record a large number of neurons simultaneously, however, it has a disadvantage of low time resolution. In this paper, we aim to discover phenomena which characterize sleep/wake states from calcium imaging data. We made an assumption that groups of neurons become active simultaneously and the neuronal activities of groups differ between sleep and wake states. We used non-negative matrix factorization (NMF) to identify those groups and their neuronal activities in time from calcium imaging data. NMF was used because neural activity can be expressed by the sum of individual neuronal activity and fluorescence intensity data are always positive values. We found that there are certain groups of neurons that behave differently between sleep and wake states.

**Keywords:** Sleep state analysis · Calcium imaging · Non-negative matrix factorization

## 1 Introduction

Sleep is controlled by the brain [9] and is essential not only for the brain to function normally but also for the survival of animals. However, the phenomenon itself is not well understood [10]. Currently, only electroencephalography (EEG), an objective method, can detect sleep/wake states (wakefulness, non-rapid-eye-movement (NREM) sleep, and rapid-eye-movement (REM) sleep), whereas behavioral methods, which record animals' posture or movement, cannot [6].


I. V. Tetko et al. (Eds.): ICANN 2019, LNCS 11727, pp. 102–113, 2019.
https://doi.org/10.1007/978-3-030-30487-4_8

EEG recordings—signals from electrodes placed on the head—reflect extracellular electrical events across the cerebral cortex (the brain surface). Therefore, the neurophysiological behavior of cortical neuronal populations are assumed to differ across sleep/wake states. Nevertheless, it is still unclear how cortical neural ensembles behave during sleep/wake states owing to the lack of measurement and analysis technology. For example, EEG recordings reflect sleep/wake states; however, individual neural activity cannot be observed using EEG. It is possible to record neural activities at the cellular level with sufficient temporal resolution using electrophysiological techniques such as patch-clamp, intracellular, and extracellular unit recordings. However, it is difficult to record a large number of neurons or identify the recorded cell types using these techniques.

To overcome the technical limitations of electrophysiological methods, we use calcium imaging techniques to observe the cortical neural activity during sleep/wake states. Calcium imaging is a technique recently developed to record neural activities at the cellular level. The fluorescence intensity of calcium indicators such as GCaMP depends on the concentration of calcium ions. It reflects the neural activity because action potential generation (spike) increases the intracellular concentration of calcium. Another characteristic of GCaMP is that it is genetically encodable and can be delivered into the target cells using virus vectors and a Cre-LoxP system. Calcium imaging in the brain can be performed in vivo with two-photon laser scanning microscopy. Calcium imaging has the disadvantage of a low time resolution (e.g., individual spikes cannot easily be captured owing to the slow kinetics and low sampling rates.); however, it has the considerable advantages of (1) high spatial resolution, (2) large recording field, and (3) ease of combination with genetic methods, where the activity of various identified neurons can be obtained simultaneously.

In this study, we aim to understand sleep/wake-dependent neural ensembles in the cerebral cortex, which hopefully increase the understanding of sleep. Calcium imaging data were acquired from identified excitatory and inhibitory neurons in layer 2/3 of the primary motor cortex (M1)—a part of the cerebral cortex—of a sleeping/waking mouse at 8 Hz. It is well known that individual neurons in the M1 exhibit sleep/wake state-dependent activity patterns [8] and the M1 contributes to memory consolidation of acquired motor skills during sleep [5]. Their population behavior during sleep/wake states, however, is still unexplored, despite its close involvement in learning and memory.

Two approaches can be considered to analyze neural ensembles; estimation of correlation and causality of neurons. We take the first approach, estimating the correlation of observed cortical neurons. To estimate causality, we need to distinguish whether a presynaptic or postsynaptic cell is fired from the data. There are studies of inference on spikes [16] and neuronal connectivity [13] from calcium imaging data. However, it is claimed in [13] that the calcium imaging data sampled with a frequency lower than 30 Hz do not provide meaningful results. Therefore, we can estimate only correlation from the calcium imaging data sampled with low frequency.

There are few reports on the statistical analysis of calcium imaging data in the brain during sleep. One example of the sleep research using calcium imaging is an analysis of neural activity in and near the lateral dorsal tegmental nucleus (LDT) of the brainstem that is a component of the REM-regulatory circuits [4]. Neuronal activity in the LDT for 20 s before and after the state transition was analyzed by a principal component analysis (PCA). Then, k-means clustering was performed for the 2D plot of the first and second principal components. A few LDT neurons were observed to be more active in the wake state than the REM state and vice versa, and all LDT neurons were less active in the NREM state than in the REM or wake states. This research indicates that neurons can be divided into a few groups and the behavior of each group differs across sleep/wake states. This study focuses on the state transition and extracted the principal components of the fluorescence intensity during state transition. However, neuronal groups throughout sleep/wake states should be analyzed for our aim.

To better understand sleep/wake-dependent neural ensembles in the cerebral cortex, we assume that groups of cortical neurons become active simultaneously and the activated groups change over time. We used non-negative matrix factorization (NMF [11]) to estimate those groups and how they are activated in time. NMF was not performed to extract the fluorescence intensity like Cox [4] did, but for the neuronal groups. We used NMF because neural activity can be expressed by the sum of individual neuronal activity; further, fluorescence intensity data are always positive values. We found that there are certain groups of neurons that behave differently between sleep and wake states.

We proposed a protocol to analyze the calcium imaging data with a low sampling rate. We showed that the well-known NMF algorithm could effectively analyze such data by comparing its performance with those of PCA and independent component analysis (ICA).

## 2 Methodology

We acquire calcium imaging data of neurons in layer 2/3 from the primary motor cortex (M1) of a sleeping/waking mouse. The imaging lasted for 15 min at 8 Hz. A total of 154 neurons were observed. The fluorescence signal in each frame for each neuron was extracted by evaluating the mean intensity of the pixels within each region of interest (ROI) after subtracting the background signal. EEG and EMG signals were also recorded during the experiments, and NREM, REM, and wake states were scored.

We made an assumption regarding the generative model of the data, which is that there are $K$ groups of observed neurons that are activated simultaneously, and the fluorescence intensity of observed neurons is generated by the combined activities of those groups. Groups can overlap and neurons can belong to multiple groups. We assume that the behavior of the groups vary over time and the activities of those groups differ between NREM, REM, and wake states. The schematic is shown in Fig. 1.

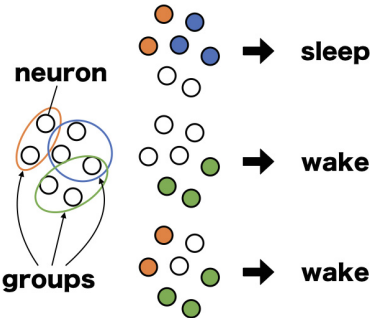


**Fig. 1.** Observed neurons are assumed to form $K$-grouped and the recorded fluorescence intensity is generated by the combined activities of those groups. In this figure, $K = 3$ groups are assumed and the activated neurons are colored.

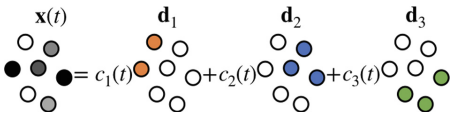


**Fig. 2.** Mathematical model designed based on the assumption Fig. 1. The fluorescence intensity of the observed neurons at time $t$, $\mathbf{x}(t)$, is represented as a weighted sum of $K$ groups $\mathbf{d}_k$. The figure shows a schematic of the model when $K = 3$.

Based on the assumption above, we designed a mathematical model for the calcium imaging data. Let $\mathbb{R}_+$ be a set of non-negative real numbers. Let $\mathbf{x}(t) \in \mathbb{R}_+^N$, $(t = 1, 2, \cdots, T)$ be the fluorescence intensity of the observed neurons at time $t$ and $\mathbf{d}_k \in \mathbb{R}_+^N$, $(k = 1, 2, \cdots, K)$ be $K$ groups of neuronal activities where $N$ is the number of observed neurons and $T$ is the observation time. Fluorescence intensity data are all positive values; therefore, $\mathbf{x}(t)$ is a positive vector. Then, $\mathbf{x}(t)$ can be modeled by the weighted sum of the groups $\{\mathbf{d}_k; k = 1, \cdots, K\}$ as follows:

$$\mathbf{x}(t) = \sum_{k=1}^{K} c_k(t)\mathbf{d}_k + \boldsymbol{\eta}(t), \tag{1}$$

where $c_k(t)$ is a positive coefficient of $\mathbf{d}_k$ and $\boldsymbol{\eta}(t) \in \mathbb{R}^N$ is a noise vector at time $t$. The schematic of the model is shown in Fig. 2. We note that the groups $\mathbf{d}_k$ are constant over time and time dependency of the observed data $\mathbf{x}(t)$ is represented by the coefficient $c_k(t)$ and noise $\boldsymbol{\eta}(t)$. The noise of calcium imaging is mostly photon shot noise, which obeys a Poisson distribution. For high photon counts, shot noise can be approximated by a Gaussian distribution [15]; therefore, $\boldsymbol{\eta}(t)$ can be represented as

$$\boldsymbol{\eta}(t) \sim \mathcal{N}(0, \sigma^2), \tag{2}$$

where $\sigma^2$ is the variance.

Equation (1) can be written in a matrix form as follows:

$$\mathbf{X} = \mathbf{DC} + \mathbf{H}, \tag{3}$$

where $\mathbf{X} \in \mathbb{R}_+^{N \times T}$, $\mathbf{D} \in \mathbb{R}_+^{N \times K}$, $\mathbf{C} \in \mathbb{R}_+^{K \times T}$, and $\mathbf{H} \in \mathbb{R}^{N \times T}$. The columns of $\mathbf{X}$ are the observation $\mathbf{x}(t)$, columns of matrix $\mathbf{D}$ are the groups $\mathbf{d}_k$, $(k, t)$-element

of matrix $\mathbf{C}$ are the coefficients $c_k(t)$, and the columns of $\mathbf{H}$ are noise vectors $\boldsymbol{\eta}(t)$. The correspondence between Eqs. (1) and (3) is shown in Fig. 3.

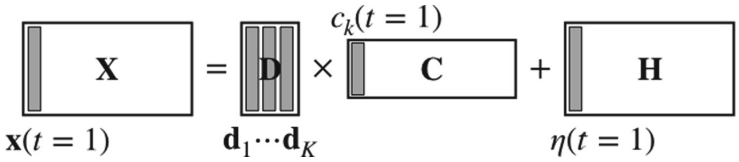


**Fig. 3.** Matrix form of Eq. (1).

We estimate the matrices $\mathbf{D}$ and $\mathbf{C}$ from the data matrix $\mathbf{X}$ by using NMF [11], which is an unsupervised learning method similar to PCA and ICA, as one of the approaches in the linear generalized component analysis [3]. NMF decomposes a non-negative matrix $\mathbf{X}$ into a product of non-negative matrices $\mathbf{D}$ and $\mathbf{C}$. By decomposing the data matrix $\mathbf{X}$ by NMF, frequent signals will be obtained as the columns of $\mathbf{D}$. The matrix $\mathbf{D}$ is called a *dictionary* in the literature of signal processing and machine learning. The columns of the dictionary $\mathbf{D}$ are interpreted as basis vectors or also called atoms. The columns of the matrix $\mathbf{C}$ are coefficients of atoms and we call $\mathbf{C}$ a coefficient matrix henceforth. Because of the non-negativity of the coefficient matrix $\mathbf{C}$, $\mathbf{X}$ is represented by a non-negative weighted sum of atoms of $\mathbf{D}$. The restriction of non-negativity also induces sparsity of $\mathbf{C}$. The number of groups $K \in \mathbb{N}$ should be given a priori for decomposition.

From Eqs. (1) to (3), $\mathbf{X}_{ij}$ is i.i.d. Gaussian random variable with mean $[\mathbf{DC}]_{ij}$ and variance $\sigma^2$:

$$p(\mathbf{X}_{ij}; [\mathbf{DC}]_{ij}) = \mathcal{N}([\mathbf{DC}]_{ij}, \sigma^2). \tag{4}$$

The dictionary $\mathbf{D}$ and coefficient matrix $\mathbf{C}$ is estimated by the following maximum log-likelihood problem under the non-negative constraints on $\mathbf{D}$ and $\mathbf{C}$:

$$\underset{\mathbf{D}\geq 0, \mathbf{C}\geq 0}{\text{maximize}} \sum_{i,j} \log p(\mathbf{X}_{ij} | [\mathbf{DC}]_{ij}). \tag{5}$$

By calculating Eq. (5), we can see that Eq. (5) is equivalent to minimizing the Frobenius norm of the difference between $\mathbf{X}$ and $\mathbf{DC}$ under the non-negative constraints on $\mathbf{D}$ and $\mathbf{C}$:

$$\underset{\mathbf{D}\geq 0, \mathbf{C}\geq 0}{\text{minimize}} ||\mathbf{X} - \mathbf{DC}||_F, \tag{6}$$

where the Frobenius norm of matrix $\mathbf{A} \in \mathbb{R}^{m \times n}$ is defined as follows:

$$||\mathbf{A}||_F = \sqrt{\sum_{i=1}^{m} \sum_{j=1}^{n} a_{ij}^2}, \quad a_{ij} \text{ is the } (i,j)\text{-element of } \mathbf{A}. \tag{7}$$

## 3 Results

We used two-photon calcium imaging data of a transgenic mouse during sleep and wakefulness. To distinguish between excitatory (glutamatergic) and inhibitory (GABAergic) neurons, Vgat-tdTomato mice were generated. Red fluorescence protein tdTomato was expressed particularly in inhibitory neurons in layer 2/3 of the M1 of Vgat-tdTomato mice, which were histologically confirmed. A genetically encoded green fluorescence calcium indicator GCaMP6s was used to monitor neural activity. GCaMP6s was delivered to M1 neurons using adeno-associated virus vectors under the control of a neuron-specific human synapsin 1 promoter. Thus, we defined GCaMP6s-positive/tdTomato-negative and GCaMP6s-positive/tdTomato-positive neurons as excitatory and inhibitory neurons, respectively. Fluorescence imaging was performed with a custom-designed upright two-photon microscope (based on Axio Examiner Z1/LSM780) and a trackball-treadmill system [10]. The mice were acclimated to sleeping on the trackball-treadmill prior to imaging experiments. GCaMP6s and tdTomato were two-photon excited at 910 and 1040 nm, respectively, using a tunable Ti:Sa laser (Maitai DeepSee, Spectra-Physics). Fluorescence of GCaMP6s and tdTomato was detected with a non-descanned GaAsP detector in the range of 500–550 nm and >555 nm, respectively (BiG, Zeiss). A 1040-nm excitation was used only to identify inhibitory neurons prior to time-lapse calcium imaging. Two-photon time-lapse images were intermittently acquired six times between 12:00 and 17:00 (the rest time for mice) at 8 frames/s with $128 \times 256$ pixels of 16-bit depth. Each imaging lasted for 15 min and we refer to each 15 min data as a dataset. EEG and EMG signals were also recorded during imaging experiments. EEG signals were amplified 40,000x and filtered with a pass-band of 0.5–500 Hz, and EMG signals were amplified 4000x and filtered with a pass-band of 1.5–1000 Hz using an analog amplifier (MEG-5200, NIHON KOHDEN). EEG/EMG signals were digitized at 2000 Hz using a 16-bit analog-to-digital converter (Digidata 1440A, Molecular Devices), and they were acquired with Clampex 10.3 software (molecular devices). Scan timing signals for two-photon imaging were also digitized with the same systems to temporally match the EEG/EMG data to the two-photon images. EEG and EMG signals were downsampled at 250 Hz, divided into 4 s epochs, and analyzed for scoring NREM/REM/wake states using a homemade Matlab program. The fluorescence signal in each frame for each neuron was extracted by evaluating the mean intensity across the pixels within each region of interest (ROI) after subtracting the background signal using Fiji/ImageJ. ROIs were set such that the neuropil signals were not included.

We calculated $\Delta F/F$ from each dataset and the data matrix $\mathbf{X}$ was created by concatenating six datasets. Then, the data matrix $\mathbf{X}$ was normalized such that the sum of each column was one. By minimizing Frobenius norm cost function, the dictionary $\mathbf{D}$ and coefficient matrix $\mathbf{C}$ were obtained. We tried 29 different values for the number of atoms $K$, increasing 10 to 150 in increments of 5, because the appropriate value for $K$ is unknown. Larger $K$ can reconstruct $\mathbf{X}$ with small error; however, the atoms would have small information. We want atoms that

have rich information; thus, we assumed a smaller $K$ than the number of neurons. We also used PCA and ICA to validate the performance of NMF.

We used random forest [1] to solve the state classification problem to compare three methods and different $K$. The input of random forest are columns of the coefficient matrix $\mathbf{C}$ for NMF. For PCA and ICA, matrices equivalent to $\mathbf{C}$ were used for the input of random forest. High accuracy in random forest means that the extracted features of the corresponding method can distinguish states. We are comparing three methods and $K$ by the accuracy of random forest. Three states, NREM, REM, and wake, were classified using 3-fold cross-validation. Train and test data were prepared after dividing the input data into 15 s blocks. The results are shown in Fig. 4. The accuracy of each validation is shown by markers, and the average of the three validations is shown by lines.

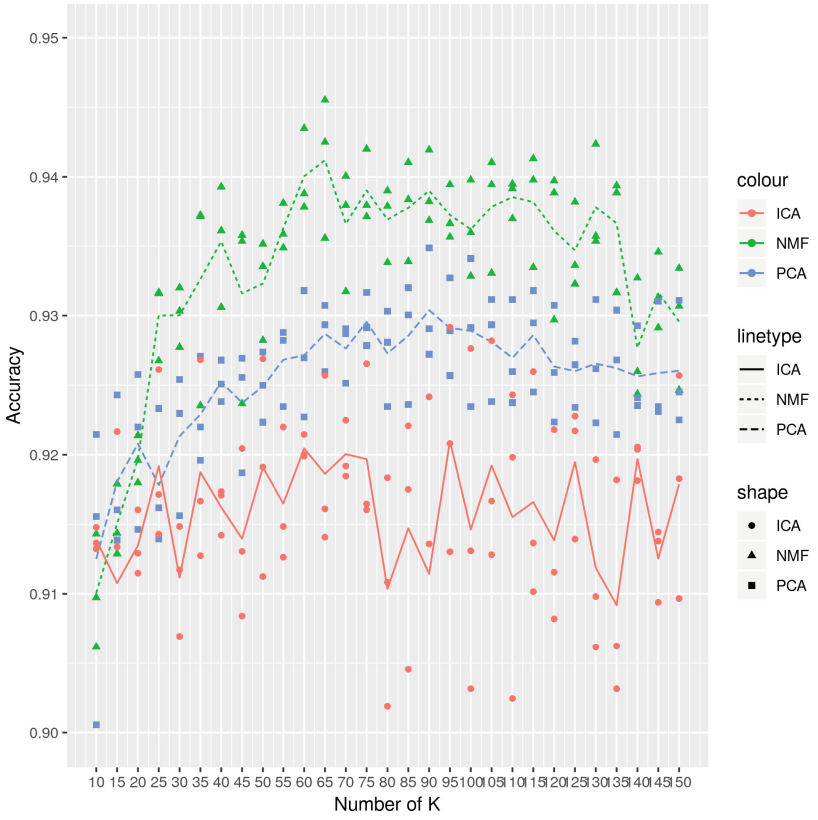


**Fig. 4.** Accuracies of state classification by the random forest with three methods and different numbers of atoms. Features used in the random forest are columns of the coefficient matrix $\mathbf{C}$ and matrices correspond to that. Three states, NREM, REM, and wake, were classified and the classification accuracy is calculated using 3-fold cross-validation. The accuracy of each validation is shown with markers and the average of three validations is shown with lines.

The result shows that NMF exhibits better performance than PCA and ICA. This suggests that NMF is more suitable for the generative process of the data with its non-negativity. The result also shows that $K = 65$ had the highest accuracy for NMF, suggesting that this is the best $K$ that extracts atoms that differ across sleep/wake states.

We then analyzed the atoms of $K = 65$. To evaluate the atoms used differently between sleep and wake states, we used the importance of random forest and Jensen–Shannon divergence [12] (JSD). We used JSD because analyzing the importance of random forest might not be sufficient. The $k$-th row of $\mathbf{C}$, $\mathbf{c}_k(t)$, is a time series of the coefficient of the atom $\mathbf{d}_k$. When values of $\mathbf{c}_k(t)$ differ between states, the corresponding atom $\mathbf{d}_k$ is considered to be used differently between states. To measure how differently an atom was used in each state, we calculated the JSD of the coefficient of each atom between NREM and wake states. REM state was not used because it rarely appears in our dataset.

The importance from random forest and the JSD of each atom are presented in Figs. 5 and 6 respectively. Top 12 atoms that had high importance and the JSD is shown in Table 1. The 58$^{\text{th}}$ atom is the highest and the 18th atom is the second highest in both importance and the JSD. However, the order of atoms after third place differed in importance and the JSD. This difference should be carefully considered; however, we could not determine the same, and thus, we would leave it for our future work.

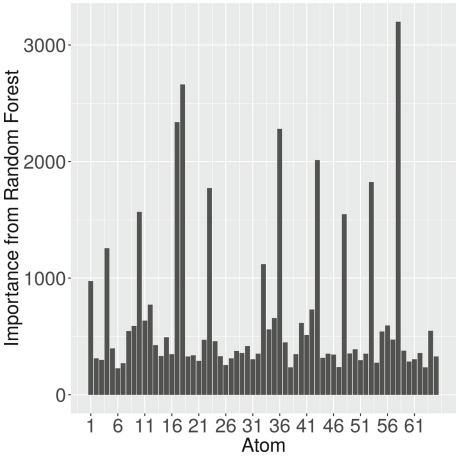


**Fig. 5.** The importance of $K = 65$ atoms from random forest.

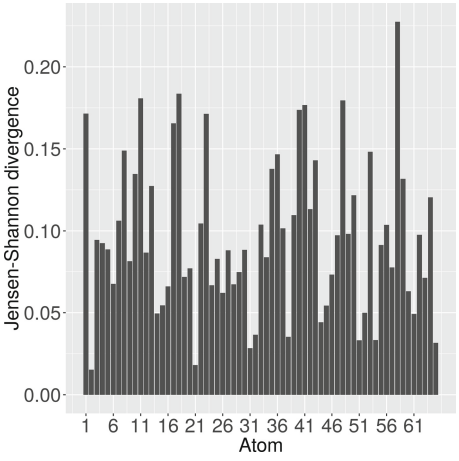


**Fig. 6.** JSD calculated from coefficients of $K = 65$ atoms.

Our aim is to analyze sleep/wake-dependent neural ensembles. Therefore, we used Otsu's method to obtain the number of neurons responsible in each atom. The result is shown in Fig. 7. Top 12 atoms from Table 1 is colored with light blue. 58$^{\text{th}}$ and 23$^{\text{rd}}$ atoms had more than 60 responsible neurons. Both atoms had high importance and the JSD.

**Table 1.** Top 12 atoms that had high importance and the JSD.

| Method | Atom | | | | | | | | | | | |
|---|---|---|---|---|---|---|---|---|---|---|---|---|
| The importance | 58 | 18 | 17 | 36 | 43 | 53 | 23 | 10 | 48 | 4 | 33 | 1 |
| JSD | 58 | 18 | 11 | 48 | 41 | 40 | 1 | 23 | 17 | 8 | 53 | 36 |

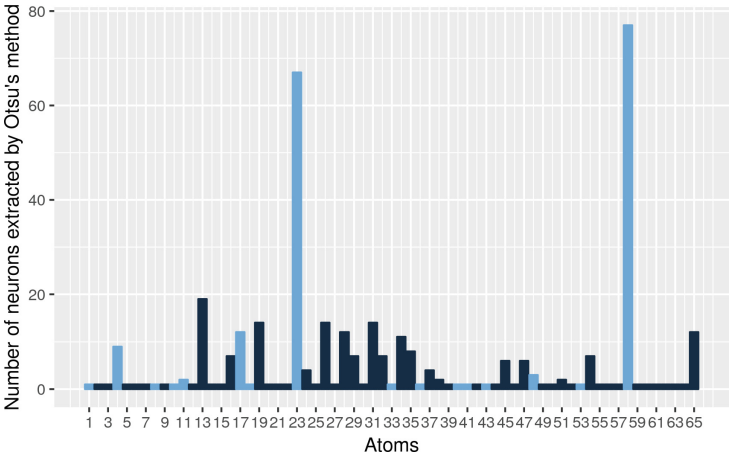


**Fig. 7.** Number of neurons responsible in each atom using Otsu's method. Top 12 atoms from Table 1 is colored with light blue. (Color figure online)

We picked up 6 atoms from Table 1 that had more than one responsible neuron. The spatial plots of those atoms are shown in Fig. 8. Red markers represent excitatory neurons and blue markers represent inhibitory neurons. The size of a marker is the intensity of the corresponding neuron. The boxplot of the coefficients of those atoms in NREM and wake is shown in Fig. 9.

From Fig. 8, $58^{\text{th}}$, $23^{\text{rd}}$, $17^{\text{th}}$, and $4^{\text{th}}$ atoms do not have evident spatial clusters; however, $48^{\text{th}}$ and $11^{\text{th}}$ atoms do. From Fig. 9, the former four atoms contribute to NREM, whereas the latter two atoms somehow contribute to wake. Co-activation of nearby neurons emerges in the M1 for stereotyped simple behaviors [7] but not for learned voluntary movements [14]. In our analysis, sleep-preferred neuronal ensembles exhibited no evident spatial clustering, suggesting that the M1 is devoted to higher-order information processing for acquiring complex behaviors during sleep.

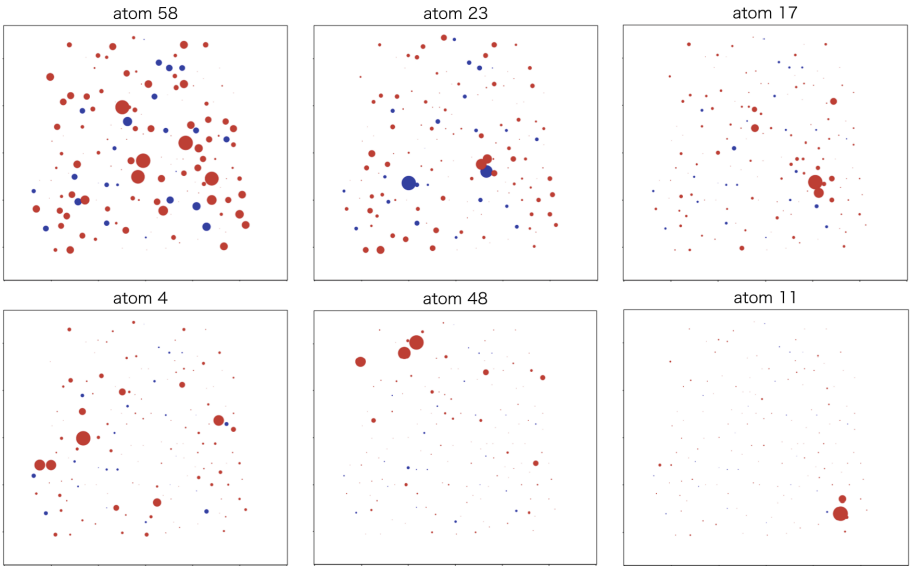


**Fig. 8.** The spatial plot of atoms. Each marker represents a neuron. The size of a marker is the intensity of the corresponding neuron.

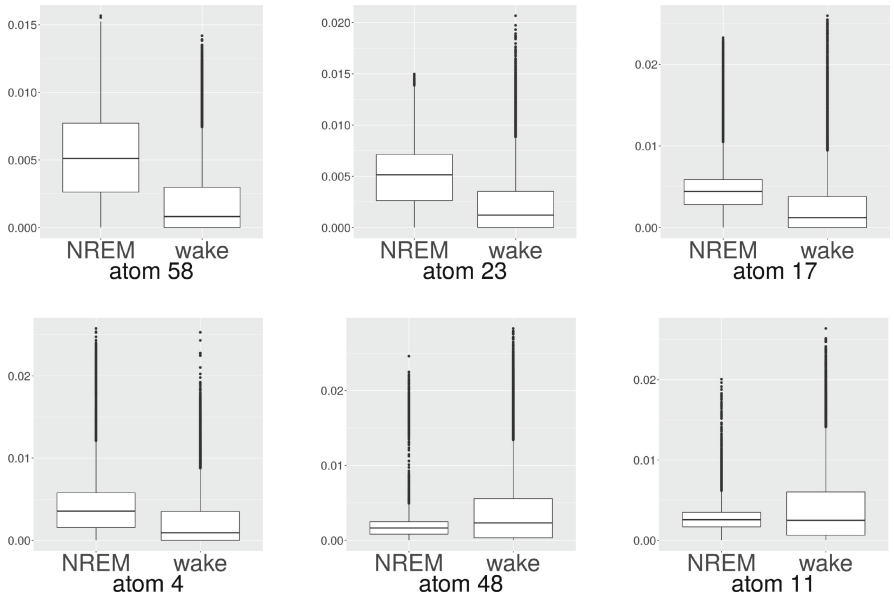


**Fig. 9.** The boxplot of the coefficients of the atoms in NREM and wake.

## 4 Conclusion

In this paper, we proposed a protocol to analyze the calcium imaging data with a low sampling rate. We decomposed the data matrix $\mathbf{X}$ with NMF and validated its performance by comparing the results obtained with those of PCA and ICA. The results showed that NMF performed better than PCA and ICA by extracting atoms whose activities differ between states. This suggests that NMF is more suitable for the generative process of the data with its non-negativity. Results also showed that there are groups of neuronal activities that become active simultaneously and some groups are related to sleep/wake states. This is a notable result because NMF does not use state information to decompose the data matrix $\mathbf{X}$. Furthermore, atoms contributing to NREM had no evident spatial clusters, which suggests that the M1 is devoted to high-order information processing for acquiring complex behavior during sleep.

For further investigation, two things should be considered. First, a method to determine the number of atoms $K$ should be developed. NMF requires that the number of atoms $K$ be determined beforehand. In this paper, we used a random forest to determine the number of atoms $K$; however, further consideration should be made from a biological perspective. Second, the characteristic of calcium imaging should be considered. Calcium imaging has a slow response to neuronal activities. The decay halftime of the calcium indicator GCaMP6s is approximately 0.5s [2], which is much higher than the sampling rate of the data we use. Therefore, we can expect better results if this property is incorporated into the decomposition model of NMF. For example, adding a constraint that makes two adjacent coefficients $c_k(t)$ and $c_k(t+1)$ similar would help effectively obtain a better dictionary $\mathbf{D}$ and its coefficient $\mathbf{C}$.

**Acknowledgements.** This work was supported by Grants-in-Aid for Scientific Research (KAKENHI), Japan Society for the Promotion of Science (JSPS) (Grant Number 16K18358 to T.K.; 26220207 to T.K. and M.Y.; 19K12111 to H.H; 17H06095 to M.Y.); World Premier International Research Center Initiative (WPI), the Ministry of Education, Culture, Sports, Science and Technology (MEXT) (to M.Y.); Core Research for Evolutional Science and Technology (CREST), Japan Science and Technology Agency (JST) (Grant Number JPMJCR1761 to H.H.; JPMJCR1655 to M.Y.); Yamada Research Grant (to T.K.), Takeda Science Foundation (to M.Y.), and Uehara Memorial Foundation (to M.Y.).

## References

1. Breiman, L.: Random forests. Mach. Learn. **45**(1), 5–32 (2001). https://doi.org/10.1023/A:1010933404324
2. Chen, T.W., et al.: Ultrasensitive fluorescent proteins for imaging neuronal activity. Nature **499**(7458), 295–300 (2013). https://doi.org/10.1038/nature12354
3. Cichocki, A., Zdunek, R., Phan, A.H., Amari, S.: Nonnegative Matrix and Tensor Factorizations. Wiley, Chichester (2009)
4. Cox, J., Pinto, L., Dan, Y.: Calcium imaging of sleep-wake related neuronal activity in the dorsal pons. Nat. Commun. **7**(1), 10763 (2016). https://doi.org/10.1038/ncomms10763

5. Dayan, E., Cohen, L.G.: Neuroplasticity subserving motor skill learning. Neuron **72**(3), 443–54 (2011). https://doi.org/10.1016/j.neuron.2011.10.008
6. Deboer, T.: Technologies of sleep research. Cell. Mol. Life Sci. **64**(10), 1227 (2007). https://doi.org/10.1007/s00018-007-6533-0
7. Dombeck, D.A., Graziano, M.S., Tank, D.W.: Functional clustering of neurons in motor cortex determined by cellular resolution imaging in awake behaving mice. J. Neurosci. **29**(44), 13751–13760 (2009). https://doi.org/10.1523/JNEUROSCI.2985-09.2009
8. Evarts, E.V.: Temporal patterns of discharge of pyramidal tract neurons during sleep and waking in the monkey. J. Neurophys. **27**, 152–71 (1964). https://doi.org/10.1152/jn.1964.27.2.152
9. Hobson, J.A.: Sleep is of the brain, by the brain and for the brain. Nature **437**(7063), 1254–1256 (2005). https://doi.org/10.1038/nature04283
10. Kanda, T., et al.: Sleep as a biological problem: an overview of frontiers in sleep research. J. Physiol. Sci. **66**(1), 1–13 (2016). https://doi.org/10.1007/s12576-015-0414-3
11. Lee, D.D., Seung, H.S.: Learning the parts of objects by non-negative matrix factorization. Nature **401**(6755), 788–791 (1999). https://doi.org/10.1038/44565
12. Lin, J.: Divergence measures based on the Shannon entropy. IEEE Trans. Inform. Theory **37**(1), 145–151 (1991). https://doi.org/10.1109/18.61115
13. Mishchencko, Y., Vogelstein, J.T., Paninski, L.: A Bayesian approach for inferring neuronal connectivity from calcium fluorescent imaging data. Ann. Appl. Stat. **5**(2B), 1229–1261 (2011). https://doi.org/10.1214/09-AOAS303
14. Peters, A.J., Chen, S.X., Komiyama, T.: Emergence of reproducible spatiotemporal activity during motor learning. Nature **510**(7504), 263–267 (2014). https://doi.org/10.1038/nature13235
15. Sjulson, L., Miesenböck, G.: Optical recording of action potentials and other discrete physiological events: a perspective from signal detection theory. Physiology **22**(1), 47–55 (2007). https://doi.org/10.1152/physiol.00036.2006
16. Vogelstein, J.T., Watson, B.O., Packer, A.M., Yuste, R., Jedynak, B., Paninski, L.: Spike inference from calcium imaging using sequential Monte Carlo methods. Biophys. J. **97**(2), 636–655 (2009). https://doi.org/10.1016/J.BPJ.2008.08.005